# All-spin-based ultrafast nanologic elements with a $Ni_4$ cluster

D. Chaudhuri, G. Lefkidis,* and W. Hübner

*Department of Physics and Research Center OPTIMAS, University of Kaiserslautern, P.O. Box 3049, 67653 Kaiserslautern, Germany*

(Received 13 July 2016; revised manuscript received 25 October 2017; published 10 November 2017)

Starting from high-level *ab initio* calculations, we present ultrafast spin dynamical effects and all-spin-based nanologic elements on a $Ni_4$ cluster. The predominant underlying mechanisms for our operations are optically induced coherent $\Lambda$ processes, the optimized parameters of which are obtained from a dedicated genetic algorithm search. The geometry of the cluster exhibits a high degree of spin localization. Thus, maneuvering the spin localizations we construct a pure-spin OR gate. Additionally, functional intramolecular cooperative effects such as spin bifurcation and spin merging are introduced that facilitate the setup of the latter. In the *which-path* information effect the phase of the final spin state is exploited to reveal the path traveled by the spin in a two-step spin transfer scenario. This is beneficial for both classical and quantum computations on small spatial and temporal scales.

DOI: 10.1103/PhysRevB.96.184413

## I. INTRODUCTION

Modern spintronics aims at miniaturizing all-spin-based devices to the atomic scale. Researchers are constantly in search of novel schemes for high-performance computing. One successful approach harnesses the spin degree of freedom of the nuclei, electrons, atoms, and molecules to perform computations [1–4]. The magnetic moment of the spin can be used to read/write information and in this way improve the performance and energy efficiency of computer hard drives and magnetic random-access-memory (MRAM) [5,6]. All electronic circuits require logic gates to perform mathematical operations. Thus, magnetic nanologic appears to be ideal due to its nonvolatile character, minimal surface area requirement, and high-speed processing.

Previously, logic operations have been performed experimentally with small molecules using input cation concentrations, and CO molecules in cascades [7,8]. Soe *et al.* developed a NOR gate using a single molecule and gold atoms to encode logical values as inputs [9]. Wang *et al.* reported quantum logic gates with a single trapped ion which eventually enhances the performance of quantum computations [10]. Logic operations have also been realized on quantum wires with external voltages as inputs and the high/low output current as the output [11]. Khajetoorians *et al.* showed that NOT and OR gates can be built by combining spin frustration and indirect exchange coupling [2]. NOR and NAND gates have been developed using three quantum states with a distance and frequency controlled approach [12]. Sequential logic operations have been reported exploiting quantum interference effects and stimulated Raman adiabatic passage on $n$-level ($n = 2,3$) systems [13]. Theoretically quantum logic has been developed using polarized photons as information carriers [14]. In thermal logic gates, the information carriers are mainly the phonons [15].

While conventional spintronics relies on spin currents, optical spin-based nanologic employs ultrafast spin dynamics and as such uses elementary excitations with large energy and small linear momentum transfer. As it is based on ultrafast laser induced $\Lambda$ processes from the outset this type of magnetic logic acts on the femtosecond timescale. In order to enhance spatial resolution, restricted by the optical diffraction limit, one needs to resort to the specific resonance structure of the different active magnetic sites (i.e., either different species or same species atoms in slightly different local geometry). Magnetic-logic operations [16–20], as well as spin processes in three-magnetic-center structures [21–23] have already been proposed. In the latter ones, however, a variable external magnetic field was used as one of the input bits [21]. This substantially slows down the operation speed.

The structural aspects of realistic magnetic systems with few magnetic centers which give rise to magnetic nanologic scenarios have already been investigated. Among others the role of correlations on the $\Lambda$ processes, the role of the different species (Ni, vs Co, vs Fe [24–26]), the role of bridging atoms (O, vs Mg, vs C, etc. [24,27]), of the geometry (linear vs bent molecules, triangles, fullerenes, planar and nonplanar geometries [28,29]), and of attached ligands (CO, ethanol, methanol, etc. [30,31]) have been studied.

In the present paper, rather than looking into those aspects, we explore the functionalities arising from using a prototypic system with four rather than three magnetic centers and develop logic elements with spins as the *only* information carriers. The infinitesimal static magnetic field used in the calculations only defines the easy axis in space. Since it has been shown that small planar structures can be stable in particular on surfaces [32–34], we concentrate here on the fundamental underlying physics and do not consider further the environmental details of such structures (studied previously, e.g., stabilizing ligands [30], attached small organic molecules like MeOH [26] and EtOH [31], or temperature [35,36]), for which it typically turns out that although the resonances might get slightly shifted, the basic physics remains the same. Especially the presence of a substrate does not alter the optical selection rules, as long as the total symmetry remains the same [37,38]. The correlations, on the other hand, open additional excitation paths and thus can give rise to further phenomena [39,40]. Although our system is spatially small it is quite huge electronically (112 electrons spanning a Hilbert space of 101 molecular orbitals and a Fock space of 24 197 many-body configurations) and has a strong open-shell character (strong

*lefkidis@physik.uni-kl.de

 

static correlations, which allow for spin-charge separation in space, i.e., static geometry, and time, i.e., dynamics). Thus high-level size-consistent quantum-chemistry methods, such as coupled-cluster methods [41], are indispensable (as seen from the following comparison with a biquadratic model Hamiltonian, of which *all* the effects are intrinsically included in our calculations).

In most molecular magnets the localization and the direction the magnetization can be coherently altered with laser pulses, and one can therefore use the latter ones to develop nanologic elements. In the quest for *all-spin based* logic elements, i.e., without the need for the active participation of a magnetic field as information carrier, a bare planar rhombic $Ni_4$ cluster is a promising candidate because of the disparate interatomic distances which facilitate the dedicated localization of the spins on each of the four magnetic centers. Tetranuclear Ni clusters and complexes have been a subject of investigation for the last decade. Kirchner *et al.* showed that the antisymmetric exchange interaction is a result of the mixing of the pseudoangular momentum and the ground state spin multiplet in $Ni_4$ clusters [42]. The electronic and magnetic properties, and the stability of different $Ni_4$ clusters, have also been investigated in the presence of other impurity atoms [43].

The rest of the paper is organized as follows. In Sec. II our theoretical results regarding the structure and its electronic-level scheme are presented (Sec. II A contains the full *ab initio* results and Sec. II B the results of a spin Hamiltonian). Section III contains our three suggested ultrafast-dynamics results, namely the elementary processes *spin-bifurcation* and *spin-merging* (Sec. III A), the *all-spin* OR gate (Sec. III B), and the *which-path-interference* effect (Sec. III C). Section IV summarizes our findings. Finally, the Appendices provide some additional information on the spin Hamiltonians regarding the formula for the biquadratic exchange interaction (Appendix A), some details of the diagonalization process (Appendix B), and the results for two electrons per site (Appendix C).

## II. THEORY

Our system of choice is $Ni_4$ in planar geometry. Generally, depending on the immediate local environment, $Ni_4$ can exist as a chain [44], a planar [45,46], or of course a tetrahedral object [42]. In order to exploit femtosecond spin dynamics to devise magnetic nanologic elements, it is important to consider not only the geometry of a bare cluster in the vacuum but a physical situation suitable for technological applications. We accomplish this by assuming the most probable conformation of the cluster when deposited on a surface, namely a two-dimensional one. Surface deposition is a way of technically tackling the challenge of the molecular orientation and geometrical stability at room temperature, present in the gas phase. From a methodological point of view before quantum mechanically describing the entirety of such systems (i.e., including surface, geometry-stabilizing ligands, and possible other air-borne adsorbents), we are interested in the proof of principles for our suggested functionalities. Therefore, in our model system we include the minimum ingredients necessary, namely a flat molecule and spin-orbit coupling for the spin dynamics, hence the choice of a bare planar structure. We

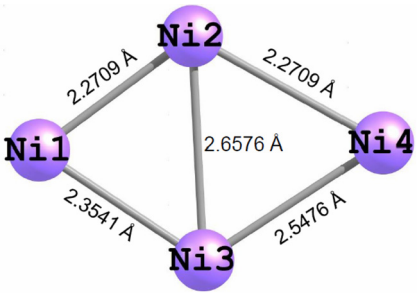


FIG. 1. Optimized structure of $Ni_4$ at the Hartree-Fock level, for which a planar geometry is imposed (see text).

treat our system in two different ways: (i) fully quantum mechanically (which we later use for our suggested ultrafast spin dynamics), in order to accurately include static and dynamic correlational effects in an *ab initio* way, and (ii) with the help of a spin Hamiltonian for comparison reasons.

### A. *Ab initio* results

Our computations are performed in four steps:

(i) Structural optimization (Fig. 1) at the Hartree-Fock (HF) level with the Los Alamos basis set with scalar relativistic effective core potentials (Ni[8s5p5d/3s3p2d]) [47]. In the optimization process we restrain ourselves to a planar geometry to mimic a surface deposited cluster.

(ii) The correlated ground and 70 many-body excited electronic states comprised of 10 singlets, 30 triplets, and 30 quintets (Fig. 2, left panel, and Table I) are computed with the symmetry-adapted cluster configuration interaction (SAC-CI) [48] method as implemented in GAUSSIAN09 [49], which includes both static and dynamic correlations [50]. The ground state is a triplet state. Table I also gives the charge and the spin density of each state, as calculated by a gross

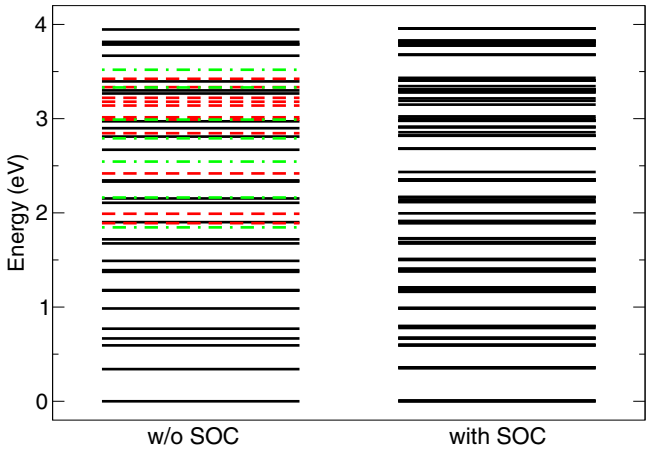


FIG. 2. Levels of the optimized $Ni_4$ as calculated with the SAC-CI method for states up to 4 eV. Left: without spin-orbit coupling, triplet states are given with the solid black lines, singlet states with the red dashed lines, and quintet states with dotted-dashed green lines. Right: after the inclusion of spin orbit coupling and restricting only to the singlet and the triplet channel (there can be no distinction between singlets and triplets after spin-orbit coupling).

TABLE I. Multiplicities, energies, charge and spin densities of all calculated electronic states of $Ni_4$ before the inclusion of spin-orbit coupling, as calculated with the SAC-CI method (see also Fig. 2, left panel). The states are organized in multiplicites first and in ascending energy then. The ground state is a triplet state. The spin density refers to the substate with the highest positive $\hat{S}_z$ eigenvalue.

| | | Charge density | | | | Spin density | | | |
|---|---|---|---|---|---|---|---|---|---|
| Multiplicity | energy (eV) | Ni1 | Ni2 | Ni3 | Ni4 | Ni1 | Ni2 | Ni3 | Ni4 |
| 1 | 1.915 | 0.021 | 0.025 | 0.108 | −0.154 | 0.000 | 0.000 | 0.000 | 0.000 |
| 1 | 2.179 | −0.065 | 0.137 | 0.252 | −0.324 | 0.000 | 0.000 | 0.000 | 0.000 |
| 1 | 2.418 | −0.156 | 0.426 | 0.023 | −0.292 | 0.000 | 0.000 | 0.000 | 0.000 |
| 1 | 2.548 | 0.036 | −0.131 | 0.202 | −0.108 | 0.000 | 0.000 | 0.000 | 0.000 |
| 1 | 2.696 | −0.280 | 0.090 | 0.262 | −0.072 | 0.000 | 0.000 | 0.000 | 0.000 |
| 1 | 3.124 | 0.219 | −0.029 | 0.128 | −0.318 | 0.000 | 0.000 | 0.000 | 0.000 |
| 1 | 3.175 | −0.530 | 0.007 | 0.311 | 0.212 | 0.000 | 0.000 | 0.000 | 0.000 |
| 1 | 3.434 | −0.215 | −0.149 | 0.401 | −0.037 | 0.000 | 0.000 | 0.000 | 0.000 |
| 1 | 3.486 | 0.125 | −0.116 | 0.334 | −0.343 | 0.000 | 0.000 | 0.000 | 0.000 |
| 1 | 3.633 | −0.265 | 0.168 | 0.292 | −0.194 | 0.000 | 0.000 | 0.000 | 0.000 |
| 3 | 0.000 | 0.016 | 0.076 | 0.125 | −0.217 | 1.736 | 0.096 | 0.120 | 0.048 |
| 3 | 0.097 | 0.034 | 0.072 | 0.126 | −0.232 | 1.765 | 0.077 | 0.110 | 0.047 |
| 3 | 0.194 | −0.052 | 0.104 | −0.000 | −0.052 | 0.005 | 0.069 | 0.207 | 1.719 |
| 3 | 0.254 | −0.069 | 0.062 | 0.027 | −0.020 | 0.031 | 0.077 | 0.179 | 1.713 |
| 3 | 0.519 | −0.055 | 0.169 | 0.175 | −0.289 | 0.037 | 0.321 | 0.448 | 1.194 |
| 3 | 0.778 | −0.092 | 0.113 | 0.329 | −0.350 | 0.111 | 0.079 | 1.487 | 0.324 |
| 3 | 0.921 | 0.050 | 0.147 | 0.067 | −0.263 | 1.403 | 0.332 | 0.186 | 0.079 |
| 3 | 1.022 | −0.044 | 0.141 | 0.292 | −0.389 | 0.160 | 0.039 | 1.552 | 0.249 |
| 3 | 1.036 | −0.176 | 0.468 | −0.025 | −0.267 | 0.155 | 1.511 | 0.230 | 0.104 |
| 3 | 1.204 | −0.144 | 0.271 | 0.117 | −0.244 | 0.107 | 1.510 | 0.208 | 0.176 |
| 3 | 1.262 | −0.429 | 0.289 | 0.308 | −0.167 | 1.015 | 0.468 | 0.443 | 0.074 |
| 3 | 1.332 | −0.174 | 0.365 | 0.118 | −0.309 | 0.518 | 1.235 | 0.130 | 0.117 |
| 3 | 1.832 | −0.084 | 0.178 | 0.248 | −0.342 | 0.081 | 0.075 | 1.219 | 0.625 |
| 3 | 2.072 | −0.025 | 0.077 | −0.108 | 0.056 | −0.017 | 0.086 | 0.521 | 1.410 |
| 3 | 2.254 | −0.051 | 0.181 | 0.068 | −0.197 | 0.055 | 0.621 | 0.423 | 0.902 |
| 3 | 2.364 | −0.055 | 0.004 | 0.230 | −0.179 | 0.567 | 0.805 | 0.244 | 0.384 |
| 3 | 2.702 | 0.020 | −0.027 | 0.191 | −0.184 | 0.241 | 0.533 | 0.355 | 0.871 |
| 3 | 2.842 | −0.386 | 0.119 | 0.157 | 0.111 | 0.465 | 0.365 | 0.467 | 0.703 |
| 3 | 3.274 | −0.068 | 0.046 | 0.077 | −0.055 | 0.279 | 0.402 | 0.599 | 0.721 |
| 3 | 3.349 | −0.050 | 0.063 | 0.266 | −0.279 | 0.247 | 0.788 | 0.482 | 0.483 |
| 5 | 1.846 | 0.267 | 0.045 | −0.066 | −0.246 | 0.333 | 0.901 | 1.358 | 1.407 |
| 5 | 2.163 | −0.215 | 0.334 | 0.133 | −0.253 | 0.818 | 0.739 | 1.093 | 1.350 |
| 5 | 2.544 | −0.239 | 0.161 | 0.188 | −0.110 | 0.955 | 0.817 | 0.720 | 1.508 |
| 5 | 2.791 | 0.325 | 0.066 | −0.191 | −0.201 | 0.370 | 1.083 | 1.090 | 1.457 |
| 5 | 2.990 | 0.346 | −0.097 | 0.302 | −0.550 | 0.854 | 1.397 | 0.946 | 0.802 |
| 5 | 3.331 | −0.101 | 0.280 | 0.134 | −0.313 | 0.756 | 0.532 | 1.039 | 1.672 |
| 5 | 3.519 | −0.284 | 0.273 | 0.133 | −0.122 | 0.780 | 0.710 | 0.870 | 1.640 |
| 5 | 4.056 | 0.166 | −0.113 | −0.111 | 0.058 | 0.495 | 1.010 | 1.335 | 1.160 |
| 5 | 4.202 | 0.175 | −0.187 | 0.167 | −0.155 | 0.519 | 1.175 | 0.979 | 1.327 |
| 5 | 4.282 | −0.140 | 0.262 | 0.340 | −0.462 | 0.954 | 0.915 | 0.793 | 1.339 |
| 5 | 4.410 | −0.223 | 0.222 | 0.137 | −0.136 | 1.055 | 0.864 | 0.861 | 1.220 |
| 5 | 4.416 | −0.248 | 0.265 | 0.153 | −0.170 | 1.118 | 0.903 | 0.893 | 1.086 |
| 5 | 4.555 | 0.043 | 0.203 | 0.230 | −0.476 | 0.950 | 0.911 | 1.003 | 1.136 |
| 5 | 4.595 | −0.269 | 0.243 | 0.380 | −0.354 | 1.215 | 0.958 | 0.745 | 1.082 |
| 5 | 4.694 | −0.322 | 0.181 | 0.266 | −0.125 | 1.004 | 0.905 | 0.730 | 1.361 |
| 5 | 4.901 | 0.261 | −0.048 | −0.103 | −0.110 | 0.345 | 0.962 | 1.391 | 1.302 |
| 5 | 5.074 | −0.389 | 0.032 | 0.301 | 0.055 | 1.126 | 1.102 | 0.904 | 0.868 |
| 5 | 5.231 | −0.091 | 0.288 | 0.150 | −0.347 | 0.748 | 0.870 | 0.900 | 1.481 |
| 5 | 5.363 | −0.206 | −0.100 | 0.286 | 0.020 | 0.999 | 1.140 | 0.876 | 0.986 |
| 5 | 5.561 | −0.328 | 0.197 | 0.388 | −0.257 | 1.310 | 0.852 | 0.713 | 1.126 |

population analysis of the reduced one-electron density matrix, in which the Slater-Condon rules are taken into account [51].

(iii) Perturbative inclusion of spin-orbit coupling (SOC) and a static external magnetic field, which defines the magnetic easy axis (Zeeman splitting). The latter is necessary both for physical and numerical reasons.

$$\hat{H}_{\mathrm{SOC}} = \sum_{i=1}^{n} \frac{Z_a^{\mathrm{eff}}}{2c^2 R_i^3} \hat{\mathbf{L}} \cdot \hat{\mathbf{S}} + \sum_{i=1}^{n} \mu_L \hat{\mathbf{L}} \cdot \mathbf{B}_{\mathrm{stat}} + \sum_{i=1}^{n} \mu_S \hat{\mathbf{S}} \cdot \mathbf{B}_{\mathrm{stat}}, \tag{1}$$

where $\hat{\mathbf{S}}$ and $\hat{\mathbf{L}}$ are the spin orbital angular momentum operators, respectively. $\mu_L$ and $\mu_S$ are their respective gyromagnetic ratios. $Z_a^{\mathrm{eff}}$ denote the relativistic effective nuclear charges which account for the two-electron contributions to the SOC. $\mathbf{B}_{\mathrm{stat}}$ is the static external magnetic field, and $c$ denotes the speed of light.

In the absence of a Zeeman splitting the spin-up and spin-down states are degenerate, and therefore any linear combination of them is an eigenstate of the total Hamiltonian, thus rendering the distinction between majority and minority spins arbitrary. This problem persists also after the inclusion of spin-orbit coupling (in which case, of course, the role of the spin $\hat{\mathbf{S}}$ is taken over by the total angular momentum $\hat{\mathbf{J}}$). Although analytically an infinitesimal magnetic field would suffice, numerically a non-negligible magnitude is needed (however, below the Paschen-Back effect limit).

Although strictly speaking, after the inclusion of spin-orbit coupling the wave functions are no longer eigenstates of the spin operator $\hat{\mathbf{S}}$, it is still possible to calculate the expectation value $\langle \hat{\mathbf{S}} \rangle$. If the electronic states are energetically isolated (that is they do not strongly interact with other electronic states), then the expectation value of the spin for these states is still close to the value without the inclusion of spin-orbit coupling. Thus we still loosely refer to them as "singlets" and "triplets."

(iv) Propagation of the wave functions under the influence of a suitably tailored laser pulse. The laser parameters are optimized with a dedicated genetic algorithm [25,52]. This heuristically searches and finds the best electronic population transfer paths within the Fock space (i.e., the many-body Hilbert space) spanned by many-body states found with our quantum chemical calculations. Although we do not impose any restriction on the order of the transitions (one-photon, two-photon, etc.) it turns out that in most relevant cases due to the selection rules the genetic algorithm suggests a $\Lambda$ process rather than direct transitions, especially whenever a spin flip is involved [53–55]. In fact there are cases in which even four-photon processes are necessary [22].

Numerically the propagation of the wave function under the influence of a $\mathrm{sech}^2$-shaped laser pulse is performed in the interaction picture. The time-dependent Hamiltonian used is

$$\hat{H}'(t) = \hat{\mathbf{D}} \cdot \mathbf{E}_{\mathrm{laser}}(t) + \mu_S \hat{\mathbf{S}} \cdot \mathbf{B}_{\mathrm{laser}}(t) + \mu_L \hat{\mathbf{L}} \cdot \mathbf{B}_{\mathrm{laser}}(t), \tag{2}$$

where $\mathbf{E}_{\mathrm{laser}}(t)$ and $\mathbf{B}_{\mathrm{laser}}(t)$ are the electric and magnetic fields of the laser pulse, respectively, and $\hat{\mathbf{D}}$ the electric-dipole-transition operator. Within the interaction picture the many-body wave function can be written as

$$\Psi(t) = \sum_n c_n(t) e^{-i E_n t/\hbar} \Psi_n \tag{3}$$

in which the coefficients $c_n(t)$ are given by the set of differential equations

$$\frac{\partial c_n(t)}{\partial t} = -\frac{i}{\hbar} \sum_k \langle \Psi_n | \hat{H}'(t) | \Psi_k \rangle c_k(t) e^{-i(E_k - E_n)t/\hbar} \tag{4}$$

which are solved numerically with an embedded fifth-order Runge-Kutta method and implementing the Cash-Karp adaptive step control [56].

It is interesting to note that the structural anisotropy of the cluster in combination with spin-orbit coupling is enough to yield spin anisotropy (and hence partial or full spin localization) despite the fact that the spin-orbit coupling term itself is isotropic. The reason is that the orbital angular momentum strongly depends on the symmetry of the whole molecule [57]. Furthermore, due to the correlations in the cluster, the wave function of each electronic state is a superposition of more than one configuration, and therefore the spin density of each atom is not a multiple of 1/2 Bohr magnetons. Here the spins are treated fully quantum mechanically and are calculated as the expectation values of the spin operators.

### B. Spin Hamiltonian

Although for our logic functionality we exclusively use the full quantum mechanical calculations, in order to better understand the level scheme of our system $Ni_4$ we also perform a series of calculations using the augmented bilinear-biquadratic Heisenberg-Dirac-van-Vleck model Hamiltonian

$$\begin{aligned} \hat{H} = &- \sum_{m>n} J_{mn} \hat{\mathbf{S}}_m \cdot \hat{\mathbf{S}}_n + \sum_{m>n} \lambda_{mn} (\hat{\mathbf{S}}_m \cdot \hat{\mathbf{S}}_n)^2 \\ &+ \sum_{m>n} \mathbf{D}_{mn} \cdot (\hat{\mathbf{S}}_m \times \hat{\mathbf{S}}_n) + \gamma \mathbf{B} \cdot \sum_m \hat{\mathbf{S}}_m, \end{aligned} \tag{5}$$

where $\hat{\mathbf{S}}_m$ is the spin operator acting on the $m$th electron of our system (i.e., the spin of the $m$th position), $J_{mn}$ and $\lambda_{mn}$ are the phenomenological linear and quadratic exchange interactions between electrons $m$ and $n$, respectively. The second summand describes the crystal shape anisotropy (similar to the zero-field splitting of spin-orbit coupling), while the third summand is the Dzyaloshinskii-Moriya interaction, which arises from the combination of superexchange interaction and spin-orbit coupling [58]. The pseudovectors $\mathbf{D}_{mn}$ phenomenologically describe the antisymmetric part of the exchange interaction. All $\mathbf{D}_{mn}$'s point perpendicular to the molecular plane and are nonzero only when the interacting electrons are along one side of the quadrilateral (almost rhombic) molecule. A symmetry-consistent way of mediating such an interaction could be through the superexchange interaction with an oxygen placed at the center [58]. $\mathbf{B}$ is an external magnetic field and $\gamma$ the gyromagnetic ratio.

Our model wave function consists of four localized spins (each on every Ni atom, see Fig. 1). The basis is

$$\begin{aligned} \psi_1 &= |\uparrow\uparrow\uparrow\uparrow\rangle \\ \psi_2 &= |\uparrow\uparrow\uparrow\downarrow\rangle \\ &\vdots \\ \psi_{16} &= |\downarrow\downarrow\downarrow\downarrow\rangle, \end{aligned} \tag{6}$$

TABLE II. Multiplicities, energies, and Dzyaloshinksii-Moriya energy splittings (up to second order) of the states of the spin Hamiltonian (5) for a perfect square with one electron per site. $J_1$ and $J_2$ are the interactions along the sides and the diagonals of the square, respectively. If biquadratic terms are considered as well, then $J_1^{(\mathrm{eff})} = J_1 - \frac{1}{2}\lambda_1$ and $J_2^{(\mathrm{eff})} = J_2 - \frac{1}{2}\lambda_2$ must substitute for $J_1$ and $J_2$ (see text). The numbers in the first column refer to the multiplicities *before* the inclusion of the Dzyaloshinksii-Moriya interaction (since after its inclusion the spins are not good quantum numbers anymore). The degeneracies refer to the energies *after* the inclusion of the interaction. The states are presented in energetic order (from higher to lower), assuming that $\xi$ and $J_m$'s are positive, and $J_1$ is slightly larger than $J_2$ (due to the different interatomic distances).

| Multiplicity | Exchange energy | Degeneracy | Dzyaloshinksii-Moriya energy |
|---|---|---|---|
| 1 | $J_1 + 2J_2$ | 1 | $-\frac{1}{2(J_1-2J_2)}\xi^2$ |
| 1 | $3J_1$ | 1 | $[\frac{1}{6J_1} + \frac{2}{3(2J_1-J_2)}]\xi^2$ |
| 3 | $J_1 + J_2$ | 2 | $-\frac{J_2}{(2J_1-J_2)(J_1+J_2)}\xi^2$ |
| | | 1 | $+\frac{3}{4}\xi - \frac{J_2}{4\left(J_1^2-J_2^2\right)}\xi^2$ |
| 3 | $J_1 + J_2$ | 2 | $-\frac{3}{4}\xi - \frac{J_2}{4\left(J_1^2-J_2^2\right)}\xi^2$ |
| | | 1 | 0 |
| 3 | $2J_1$ | 2 | $[\frac{1}{8J_1} + \frac{1}{4(J_1-J_2)}]\xi^2$ |
| | | 1 | $\frac{1}{2(J_1-2J_2)}\xi^2$ |
| 5 | 5 | 2 | $-\frac{3}{6}\frac{J_1-J_2}{J_1(J_1+J_2)}\xi^2$ |
| | | 2 | $-\frac{3}{8}\frac{J_1-J_2}{J_1(J_1+J_2)}\xi^2$ |
| | | 1 | 0 |

where each arrow represents an up or down electron. The bilinear term of Eq. (5) can be easily calculated analytically for the case of a perfect square. By setting $J_1 \equiv J_{12} = J_{24} = J_{34} = J_{13}$ and $J_2 \equiv J_{14} = J_{23}$ one gets

$$\hat{H} = -J_1(\hat{\mathbf{S}}_1 \cdot \hat{\mathbf{S}}_2 + \hat{\mathbf{S}}_2 \cdot \hat{\mathbf{S}}_4 + \hat{\mathbf{S}}_3 \cdot \hat{\mathbf{S}}_4 + \hat{\mathbf{S}}_1 \cdot \hat{\mathbf{S}}_3) - J_2(\hat{\mathbf{S}}_1 \cdot \hat{\mathbf{S}}_4 + \hat{\mathbf{S}}_2 \cdot \hat{\mathbf{S}}_3) \quad (7)$$

The numbering is according to Fig. 1. By coupling $\hat{\mathbf{S}}_1$ and $\hat{\mathbf{S}}_4$ to $\hat{\mathbf{S}}_a$, $\hat{\mathbf{S}}_2$ and $\hat{\mathbf{S}}_3$ to $\hat{\mathbf{S}}_b$, and then $\hat{\mathbf{S}}_a$ and $\hat{\mathbf{S}}_b$ to the total $\hat{\mathbf{S}}$, the above equation becomes

$$\hat{H} = -J_1\hat{\mathbf{S}}_a \cdot \hat{\mathbf{S}}_b - J_2\left(\hat{\mathbf{S}}_1 \cdot \hat{\mathbf{S}}_4 + \hat{\mathbf{S}}_2 \cdot \hat{\mathbf{S}}_3\right) = -\frac{J_1}{2}\left(S^2 - S_a^2 - S_b^2\right) - \frac{J_2}{2}\left(S_a^2 + S_b^2 - 3\right), \quad (8)$$

where we used $\left(\hat{\mathbf{S}}_m + \hat{\mathbf{S}}_n\right)^2 = S_m^2 + S_n^2 + 2\hat{\mathbf{S}}_m \cdot \hat{\mathbf{S}}_n$ for $m \neq n$ and $S_m^2 = S_n^2 = \frac{3}{4}$ for one electron per site.

For one electron per site one can get rid of the biquadratic term by using an effective bilinear term $J_{mn}^{(\mathrm{eff})} = J_{mn} - \frac{1}{2}\lambda_{mn}$ (see also Appendix A and Ref. [59]). This reduction is possible due to the specific dimensionality (three) of the SU(2) Lie group. All in all, as it turns out, the biquadratic term does not change the form of the solutions (see first two columns of Table II).

For positive $J_{ij}$'s, Eq. (5) yields a quintet ground state, as well as three triplet and two singlet excited states. In the case of a square planar structure (i.e., symmetry point group $C_{4v}$) two of the triplets are degenerate. This degeneracy is lifted if the diagonal couplings are not equal ($J_{14} \neq J_{23}$), as would be the case for a rhombic molecule. These results differ substantially from the *ab initio* ones, which yield a triplet ground state. The reason is that in the latter the spatial part of the wave function also contributes to the energies of the electronic states and, due to the specific local geometry, the unpaired $d$ electrons are no longer degenerate.

An interesting fact is that the composition of the triplets is not the same. While in the nondegenerate case both diagonal pairs are triplets (i.e., $S_a^2 = S_b^2 = 2$), in the two degenerate ones the one is a singlet and the other a triplet (i.e., $S_a^2 = 0$ and $S_b^2 = 2$, or $S_a^2 = 2$ and $S_b^2 = 0$). This means that in the first case the spin density is equally distributed among *all* four atoms, while in the second one the spin density is distributed *only* among two diagonally lying atoms. As it turns out in the real quantum-chemistry calculations, those states are necessary for the implementation of spin logic. The also necessary states, for which the spin is localized on only one Ni atom do not exist, unless the symmetry is further broken (going to a rhombic or kitelike molecule is not enough).

Once we add the Dzyaloshinkii-Moriya term it is no longer possible to diagonalize Eq. (5) analytically but only perturbatively (Table II, last column). The quintet subspace splits in $2 \oplus 2 \oplus 1$ blocks, and the triplets in $2 \oplus 1$ blocks, as expected due to the Kramers' degeneracy theorem. It is interesting that also the degeneracy between the two energetically lower triplets gets lifted, since they interact with each other. In fact, this is the only first-order Dzyaloshinskii-Moriya energy correction (see Appendix B for details). The reader should bear in mind, however, that this interaction is intrinsically different from the pure spin-orbit interaction, in that it does not change the dimension of the total Hilbert space like the latter one does (which multiplies the dimension of the spin degeneracy with the dimension of the orbital-angular-momentum degeneracy).

Introducing geometry distortions also lifts the triplet-triplet degeneracy. The energy difference between the lowest triplet and the lowest singlet (which is connected to the exchange interaction) approaches 2.0 eV (the value computed with the full *ab initio* SAC-CI method) for $J_{ij} \approx 0.13$ eV. A simple approach to derive the exchange integrals is to calculate the energies of the lowest singlet and the lowest triplet state of $Ni_2$ with the interatomic distances of Fig. 1, resulting in the following matrix (all values are in eV)

$$\mathbf{J} = \begin{pmatrix} 0.00000 & 0.00570 & 0.00830 & 0.00000 \\ 0.00570 & 0.00000 & 0.01197 & 0.01197 \\ 0.00830 & 0.01197 & 0.00000 & 0.01140 \\ 0.00000 & 0.01197 & 0.01140 & 0.00000 \end{pmatrix}. \quad (9)$$

These values, however, deviate substantially from the empirical value needed to even resemble the actual level scheme (the values are in eV). The values needed are approximately $J_1 = 1.9$ eV along the side and $J_2 = 2.25$ eV diagonally. As a comparison we also mention the values of 0.99 eV for onsite exchange interaction in ferromagnetic Ni [60] and 0.3 eV for the exchange-split energy-band dispersion near the $L$ edge [61]. This discrepancy is attributed to the fact that the spin Hamiltonian does not take into account the chemical bonds built by the spatial part of the wave functions and thus assumes faulty orbital degeneracies [62]. Another reason is the absence of correlations (both static and dynamic).

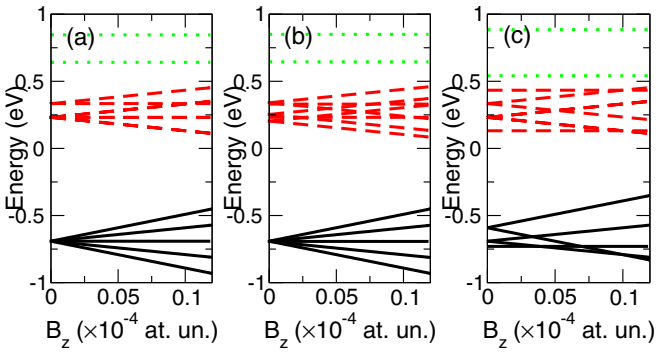


FIG. 3. Level scheme of the model Hamiltonian as a function of an external magnetic field. There is one quintet (solid black lines), three triplets (dashed red lines), and two singlets (dashed green lines). (a) Only isotropic bilinear and biquadratic exchange interaction terms, (b) isotropic bilinear and biquadratic exchange plus Dzyaloshinksii-Moriya interaction terms, (c) anisotropic bilinear, biquadratic, and Dzyaloshinskii-Moriya terms. The symmetry reduction (and hence the level splitting) of the anisotropic bilinear and the Dzyaloshinksii-Moriya term are similar in nature but significantly differ in magnitude.

A symmetry-conforming zero-field splitting can also be achieved by introducing an anisotropic exchange interaction $J_{ij}^{(x)} = J_{ij}^{(y)} \neq J_{ij}^{(z)}$ [compare Figs. 3(b) and 3(c)]. Then the first summand of Eq. (5) becomes $-\sum_{\substack{i>j \\ k=x,y,z}} J_{ij}^{(k)} S_i^{(k)} S_j^{(k)}$, which at first glance yields a splitting similar to the Dzyaloshinskii-Moriya. There are, however, two substantial differences: (a) the anisotropic exchange, being a first-order effect yields a much larger splitting, and (b) it has a predefined spatial direction, in other words the magnitude of the splitting depends on the angle of the applied B field (not shown here). This allows for additional control of the magnetic properties of the system through the external magnetic field and the derivation of magnetic logic operations [21].

If we compare these results with the ones of the full *ab initio* calculations, we see that there are substantial differences, which cannot be bridged no matter what exchange parameters are chosen. The one is the number of states (16 for the model Hamiltonian vs 40 of the SAC-CI method). The second is that the model Hamiltonian cannot yield correct energies, because (i) it does not take electronic correlations into account, and (ii) it assumes that the exchange integrals have the same values for all electronic states regardless of their spatial composition, something that is not the case as has been shown both theoretically [63] and experimentally [64].

## III. QUANTUM LOGIC

All the results in this section are based on the *ab initio* calculations and *not* on the model Hamiltonian. Since we are interested in states which exhibit strong spin localization, in the following we focus on the triplets, since the singlets have no spin density, while in the quintets, at least for the energetically lower lying ones, the spin density is always equally divided among all atoms. The reason is that the higher the multiplicity, the stronger the tendency of the electrons to avoid each other is (because high multiplicity implies electrons with parallel spin). The basic block of our magnetic logic are laser-induced $\Lambda$ processes, in which a suitable laser pulse either transfers the spin density from one atom to another or it flips it (spin-up to spin-down and vice versa). [54,55,65,66]. The reader should keep in mind that here the notions "spin localization" and "spin orientation" do not refer to classical spins but to the spin density localization and the relative magnitudes of the quantum mechanical spin operators $\langle \hat{S}_x \rangle$, $\langle \hat{S}_y \rangle$, and $\langle \hat{S}_z \rangle$, respectively.

### A. Elementary processes

As it has already been shown before, logic operations must at least include both spin flip and spin transfer between the different Ni atoms [21,24,30,35]. The local symmetry of the magnetic centers differs enough to allow for spin localization and individual behavior but is similar enough so that they exhibit combined spin dynamics [27]. For spin flip the initial and final states are usually substates of the same triplet and thus quasidegenerate. Being localized on the same atom, however, they cannot be used for spin transfer. The obligatory choice of substates of different triplets renders the relevant $\Lambda$ processes nontrivial [31,55]. Furthermore, an intermediate excited state which is optically addressable from both triplet states is needed. Intermediate states are generally spin mixed states (although strictly mathematically speaking for spin transfer this needs not be the case). The spin mixing mechanism is SOC and the external B field. The degree of spin localization is calculated with Mulliken population analysis of the reduced one-electron density matrix. Table III summarizes the energies, spin angular momentum components, as well as the spin localization of the states considered here.

TABLE III. Energies and expectation values of the spin angular momentum components for the spin manipulation scenarios in $Ni_4$ for the relevant many-body states with spin-orbit coupling included.

| | | | | | Spin density | | | | | |
|---|---|---|---|---|---|---|---|---|---|---|
| State | E (eV) | $\langle S_x \rangle$ | $\langle S_y \rangle$ | $\langle S_z \rangle$ | Ni1 | Ni2 | Ni3 | Ni4 | Localization | Functionality |
| $\|14\rangle$ | 0.79 | 0.33 | −0.00 | −0.41 | 0.032 | 0.307 | 0.685 | 2.541 | Ni4 | transfer |
| $\|15\rangle$ | 0.79 | 0.33 | 0.05 | 0.42 | 0.033 | 0.311 | 0.654 | 2.724 | Ni4 | merging |
| $\|16\rangle$ | 0.98 | −0.39 | −0.00 | 0.41 | 0.184 | 0.321 | 2.168 | 0.635 | Ni3 | transfer |
| $\|23\rangle$ | 1.66 | 0.38 | 0.05 | −0.30 | 0.263 | 1.387 | 1.623 | 0.481 | N2i+Ni3 | bifurcation/merging |
| $\|25\rangle$ | 1.37 | −0.44 | 0.01 | −0.24 | 1.248 | 1.119 | 0.999 | 0.283 | Ni1 | bifurcation |
| $\|51\rangle$ | 2.34 | −0.76 | 0.00 | −0.211 | 0.895 | 0.282 | 0.083 | 0.322 | Ni1 | transfer |
| $\|54\rangle$ | 2.35 | −0.76 | 0.00 | −0.04 | 0.575 | 0.745 | 0.304 | 0.473 | Ni2 | transfer |
| $\|58\rangle$ | 2.68 | 0.33 | 0.00 | −0.71 | 0.317 | 0.800 | 0.514 | 0.289 | Ni2 | transfer |
| $\|61\rangle$ | 2.82 | −0.01 | 0.00 | −0.82 | 0.562 | 0.385 | 0.491 | 1.088 | Ni4 | transfer |

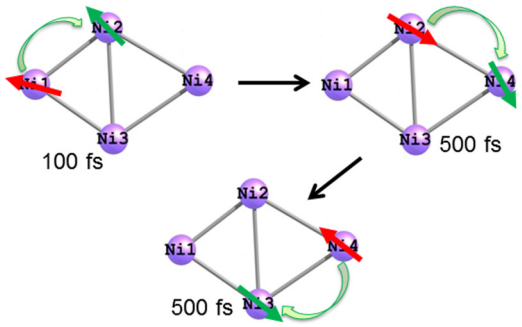


FIG. 4. Schematic showing a series of spin transfer scenarios between the magnetic centers along with the transition time for the processes. The red and the green arrows indicate the initial and the final states, respectively. The arrows do not refer to classical spins; they merely visualize the spin-density localization of the quantum mechanical spin operators $\langle \hat{S}_x \rangle$, $\langle \hat{S}_y \rangle$, and $\langle \hat{S}_z \rangle$.

Once the spin-density localization is established, three direct spin-transfer scenarios (Ni1 $\rightarrow$ Ni2, Ni2 $\rightarrow$ Ni4, and Ni4 $\rightarrow$ Ni3) are obtained (Fig. 4). For brevity we only discuss the Ni1 $\rightarrow$ Ni2 transfer process where $|51\rangle$ and $|54\rangle$ are the initial and final states, with energies $E_{|51\rangle} = 2.342$ eV and $E_{|54\rangle} = 2.354$ eV, respectively. There are two prominent intermediate states, the ground state $|1\rangle$ and state $|56\rangle$ with energy $E_{|56\rangle} = 2.356$ eV. The magnitude of the external **B** field is 2.35 T and is directed along the $x$ axis of the molecule [Fig. 1(a)]. Optimization of the linearly polarized pulse which drives the transfer yields: $\theta = 216.422^\circ$, $\phi = 264.433^\circ$, $\xi = 90.088^\circ$, $I = 2.352$ J/(sm$^2$), $FWHM = 109$ fs, and $E_\omega = 2.397$ eV (Table IV). The details of the laser parameters can be found elsewhere [26]. This spin transfer finishes within 100 fs and is five times faster than the other spin transfer scenarios in the molecule. Spin flips on each of the four centers were also found.

In the present study we present two functional intramolecular effects namely *spin bifurcation* and *spin merging*, which require a minimum of four active centers. For brevity we only discuss the dynamics for the former (Fig. 5) and list the optimized laser parameters for the latter in Table IV.

In Fig. 5(a) a linearly polarized laser pulse induces a spin transfer from Ni1 ($|25\rangle$) to Ni2 and Ni3 ($|23\rangle$). Almost 75% of the total population can be transferred to $|23\rangle$ (final state), 15% of the population remains in $|25\rangle$. The rest mainly remains in states $|26\rangle$ and $|27\rangle$ (the prominent intermediate states of the transfer process). An in-plane, static external **B** field of 4.70 Tesla is applied ($\theta = 90^\circ$ and $\phi = 30^\circ$ in spherical coordinates). The change in the expectation values of the components of spin angular momentum is shown in Fig. 5(b), and the optimized laser parameters are listed in Table IV. The energy difference $\Delta E_{|25\rangle \rightarrow |23\rangle} = 0.173$ eV is off-resonant with the laser pulse (0.169 eV), making the population transfer highly oscillatory. A sketch of the spin bifurcation scenario is shown in Fig. 5(d).

Spin merging is the reverse of spin bifurcation. In this case, with proper choice of initial ($|23\rangle$) and final ($|15\rangle$) states the spins localized on Ni2 and Ni3 are transferred to Ni4 when the system is driven by a laser pulse. The energies and expectation values of the involved states are summarized in Table III; the laser pulse is given in Table IV.

### B. *All-spin* OR gate

Utilizing the spin-transfer, spin-bifurcation, and spin-merging scenarios we construct an *all-spin* OR gate. An active center has the bit value 1 if it carries at least 50% of the total spin density and 0 otherwise. Ni2 and Ni3 carry the input bits while Ni4 is the output bit. Ni1 hosts an auxiliary (storage) bit which, without itself taking part in the logic operation, accommodates the spin when both input and output bits are 0 so that the total spin remains conserved (since we are dealing with reversible optical processes we can only construct entropy-conserving, Toffoli-like gates [67]). Figure 6 and Table IV summarize the four physical situations encoding the logical operations of the OR gate. These spin-transfer scenarios are necessary and sufficient for establishing a complete Boolean logic and thus enabling digital information processing in future optical computers.

In Fig. 6(a), the spin is localized on Ni1 in the state $|51\rangle$ (Table III). Since no spins are localized on Ni2 and Ni3, the inputs bits A and B are 0 (Table V). A laser pulse can never directly transfer the spin to Ni4, thus the output bit Q at Ni4 remains 0.

In Fig. 6(b) spin is localized on Ni2. Thus we assign values of A=1 and B=0, respectively, to the initial state (Table V). A linearly polarized laser pulse transfers the spin to Ni4 (Table III) which then carries the output bit value Q=1. Similarly, in Fig. 6(c) the spin is transferred from Ni3 $\rightarrow$ Ni4. The respective logical values are A=0 and B=1 before, and the output Q=1 at Ni4 after the pulse (Table V). This is the opposite spin transfer process to the scenario shown in Fig. 4.

Lastly, Fig. 6(d) represents the spin-merging process. From Table III, we see that the spin of state $|23\rangle$ is equidistributed between Ni2 and Ni3. Therefore, we assign the value 1 to both inputs A and B. A laser pulse can now transfer the spin to Ni4 yielding the output Q=1. Thus, the complete OR truth table is established. We emphasize again, that here only spins carry

TABLE IV. The optimized laser parameters for the spin manipulation scenarios in $Ni_4$.

| States $\|i\rangle \rightarrow \|f\rangle$ | $\theta$ (°) | $\phi$ (°) | $\xi$ (°) | Intensity (Js$^{-1}$m$^{-2}$) | FWHM (fs) | Energy (eV) | Localization | Process |
|---|---|---|---|---|---|---|---|---|
| $\|51\rangle \rightarrow \|54\rangle$ | 216.42 | 263.43 | 90.09 | 2.35 | 109 | 2.39 | Ni1 $\rightarrow$ Ni2 | spin-transfer |
| $\|58\rangle \rightarrow \|61\rangle$ | 0.00 | 64.05 | 25.69 | 0.59 | 300 | 2.67 | Ni2 $\rightarrow$ Ni4 | spin-transfer |
| $\|14\rangle \rightarrow \|16\rangle$ | 22.52 | 219.59 | 252.67 | 0.22 | 153 | 1.76 | Ni4 $\rightarrow$ Ni3 | spin-transfer |
| $\|25\rangle \rightarrow \|23\rangle$ | 104.52 | 212.90 | 52.43 | 0.57 | 53 | 0.17 | Ni1 $\rightarrow$ Ni2+Ni3 | spin-bifurcation |
| $\|23\rangle \rightarrow \|15\rangle$ | 77.77 | 351.55 | 73.55 | 0.15 | 63 | 0.37 | Ni+Ni3 $\rightarrow$ Ni4 | spin-merging |

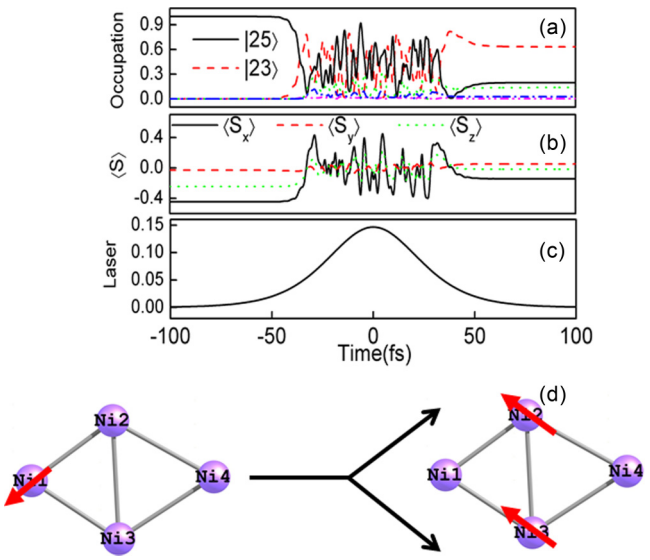


FIG. 5. Spin bifurcation scenario in $Ni_4$. (a) Population transfer from the initial state $|25\rangle$ (solid black) to the final state $|23\rangle$ (dashed red). (b) The time-resolved spin expectation values. (c) Envelope of the optimized laser pulse. (d) Schematic of the spin-bifurcation scenario. The arrows do not refer to classical spins; they merely visualize the spin density localization of the quantum mechanical spin operators $\langle\hat{S}_x\rangle$, $\langle\hat{S}_y\rangle$, and $\langle\hat{S}_z\rangle$.

information (contrary to previous work where the external magnetic field also coded an input bit [21]). This forms the basis for classical computation.

A minor yet important detail is that the lifetime of the relevant states must be longer than the gate operation time [21]. According to the DiVincenzo critieria a fault-tolerant error correction is possible if the decoherence time is four orders of magnitude longer than the clock time [68]. In this respect, molecular systems are clearly in advantage due to the absence of conformational changes [69]. As an example, we mention the $Cr_7Ni$ and $Cr_7Mn$ heterometallic wheels, the experimentally measured spin relaxation times of which are of

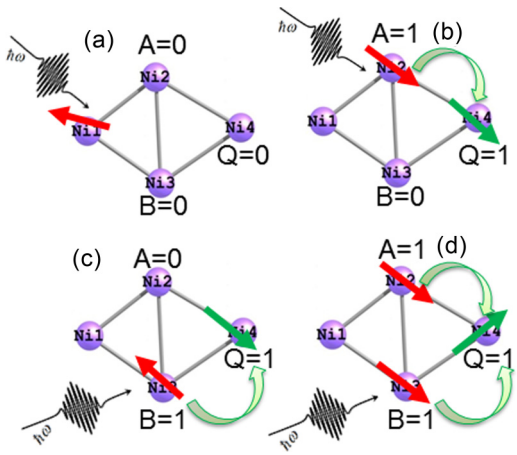


FIG. 6. Schematic of the molecular OR gate. Logic values A and B are the inputs at Ni2 and Ni3 and Q=A ∪ B is the logical output at Ni4. The arrows do not refer to classical spins; they merely visualize the spin density localization of the quantum mechanical spin operators $\langle\hat{S}_x\rangle$, $\langle\hat{S}_y\rangle$, and $\langle\hat{S}_z\rangle$.

TABLE V. Truth table for the proposed molecular OR gate.

| Laser | Ni2 A | Ni3 B | Ni4 Q=A ∪ B | fidelity | Figure |
|---|---|---|---|---|---|
| $l_1$ | 0 | 0 | 0 | | Fig. 6(a) |
| $l_2$ | 1 | 0 | 1 | 97% | Fig. 6(b) |
| $l_3$ | 0 | 1 | 1 | 60% | Fig. 6(c) |
| $l_4$ | 1 | 1 | 1 | 84% | Fig. 6(d) |

the order of microseconds [70]. Theoretical studies show that the longitudinal relaxation time $T_1$ and transverse relaxation time $T_2$ are calculated to be about 10 times slower if they are mediated through phonons than through laser pulses in a $Ni_3Na_2$ cluster [35], and some of the energetically lower-lying electronic states have about two orders of magnitude longer lifetimes than our Λ processes, because the relaxation relevant transitions are either Laporte- or spin-forbidden [30].

TABLE VI. Multiplicities, degeneracies, and energies of the states of the spin Hamiltonian (5) for a perfect square with two electrons per site (for a comparison with other geometries see also Ref. [72]). $J_0$ is the intrasite interaction, $J_1$ and $J_2$ are the interactions along the sides and the diagonals of the square, respectively. If biquadratic terms are considered as well, then $J_0^{(\mathrm{eff})} = J_0 - \frac{1}{2}\lambda_0$, $J_1^{(\mathrm{eff})} = J_1 - \frac{1}{2}\lambda_1$, and $J_2^{(\mathrm{eff})} = J_2 - \frac{1}{2}\lambda_2$ must substitute for $J_0$, $J_1$, and $J_2$ (see text). The states are order first in ascending multiplicities and then in ascending energies assuming $J_0 > J_1 > J_2$.

| Multiplicity | Degeneracy | Energy |
|---|---|---|
| 1 | 1 | $10J_1$ |
| 1 | 1 | $6J_1 - 4J_2$ |
| 1 | 1 | $4J_1 - 6J_2$ |
| 1 | 4 | $J_0 + 6J_1 - 3J_2$ |
| 1 | 2 | $2J_0 + 4J_1 - 4J_2$ |
| 1 | 4 | $2J_0 + 6J_1 - 2J_2$ |
| 1 | 1 | $4J_0 + 4J_1 - 2J_2$ |
| 3 | 1 | $9J_1$ |
| 3 | 2 | $7J_1 - 2J_2$ |
| 3 | 1 | $5J_1 - 4J_2$ |
| 3 | 2 | $4J_1 - 5J_2$ |
| 3 | 4 | $J_0 + 7J_1 - J_2$ |
| 3 | 4 | $J_0 + 5J_1 - 3J_2$ |
| 3 | 4 | $J_0 + 4J_1 - 4J_2$ |
| 3 | 2 | $2J_0 + 4J_1 - 3J_2$ |
| 3 | 4 | $2J_0 + 5J_1 - 2J_2$ |
| 3 | 4 | $3J_0 + 4J_1 - 2J_2$ |
| 5 | 1 | $7J_1$ |
| 5 | 2 | $5J_1 - 2J_2$ |
| 5 | 1 | $3J_1 - 4J_2$ |
| 5 | 2 | $4J_1 - 3J_2$ |
| 5 | 4 | $J_0 + 5J_1 - J_2$ |
| 5 | 4 | $J_0 + 3J_1 - 3J_2$ |
| 5 | 2 | $2J_0 + 4J_1 - J_2$ |
| 5 | 4 | $2J_0 + 3J_1 - 2J_2$ |
| 7 | 1 | $4J_1$ |
| 7 | 2 | $2J_1 - 2J_2$ |
| 7 | 4 | $J_0 + 2J_1 - J_2$ |
| 9 | 1 | 0 |

### C. *Which-path* interference

The combination of bifurcation and merging also gives rise to one additional effect, which can be exploited for quantum computations, namely the *which-path-interference* effect, in which the path traveled by the spin can be traced back owing to its phase. As an example we consider here the spin transfer from Ni1 to Ni4, following two different paths: (a) via one single atom Ni1 $\rightarrow$ Ni2 $\rightarrow$ Ni4, and (b) via two atoms Ni1 $\rightarrow$ Ni2+Ni3 $\rightarrow$ Ni4 (bifurcation and merging). We look at the phase of the final state after the two laser pulses, which drive the spin along the two different paths. For path (a), i.e., $|51\rangle \rightarrow |54\rangle \rightarrow |61\rangle$ with fidelities 83.3% and 91.3% for the two partial transfers, the spin of the final state gets phase shifted by about $\frac{\pi}{4}$ with respect to the initial state. For path (b), i.e., $|25\rangle \rightarrow |23\rangle \rightarrow |15\rangle$ with fidelities 63.4% and 77.2% for the bifurcation and the merging, respectively, the phase shift of the final state is $\frac{3\pi}{2}$. The procedure is analogous to Young's two-slit type interference experiments where the relationship between fringe visibility (phase essentially) and *which-path* information can be traced back depending on the path traversed by the photon [71].

## IV. CONCLUSIONS

Summarizing our findings on $Ni_4$ we find: (i) High-level *ab initio* calculation indicates a quasirhombic structure. (ii) Besides laser-induced local spin flip and spin transfer between adjacent atoms, the four magnetic atoms give rise to two functionalities, i.e., spin-bifurcation and spin-merging. (iii) We were able to construct a pure-spin OR gate, which means that four-center structures are sufficient for ultrafast, magnetic, classical-logic elements. And (iv) by using the different spin-transfer paths, we detect a *which-path-intereference effect*, in which the total phase shift of the final spin state reveals the exact path followed. The present study serves as a proof-of-principles of the logic functionalities arising from structures with four magnetic centers and can help pave the way towards the design of nanospintronics applications.

## ACKNOWLEDGMENT

The authors acknowledge funding from the German Research Foundation (Deutsche Forschungsgemeinschaft, DFG) via the Transregional Collaborative Research Center SFB/TRR 88 "3MET".

## APPENDIX A: BIQUADRATIC EXCHANGE INTERACTION

The biquadratic exchange interaction between two electrons $m$ and $n$ is proportional to

$$\begin{aligned}
\left(\hat{\mathbf{S}}_m \cdot \hat{\mathbf{S}}_n\right)^2 &= \left(\hat{S}_m^{(x)}\hat{S}_n^{(x)} + \hat{S}_m^{(y)}\hat{S}_n^{(y)} + \hat{S}_m^{(z)}\hat{S}_n^{(z)}\right)^2 \\
&= \left(\hat{S}_m^{(x)}\right)^2\left(\hat{S}_n^{(x)}\right)^2 + \left(\hat{S}_m^{(y)}\right)^2\left(\hat{S}_n^{(y)}\right)^2 + \left(\hat{S}_m^{(z)}\right)^2\left(\hat{S}_n^{(z)}\right)^2 + \hat{S}_m^{(x)}\hat{S}_n^{(x)}\hat{S}_m^{(y)}\hat{S}_n^{(y)} + \hat{S}_m^{(x)}\hat{S}_n^{(x)}\hat{S}_m^{(z)}\hat{S}_n^{(z)} \\
&\quad + \hat{S}_m^{(y)}\hat{S}_n^{(y)}\hat{S}_m^{(x)}\hat{S}_n^{(x)} + \hat{S}_m^{(y)}\hat{S}_n^{(y)}\hat{S}_m^{(z)}\hat{S}_n^{(z)} + \hat{S}_m^{(z)}\hat{S}_n^{(z)}\hat{S}_m^{(x)}\hat{S}_n^{(x)} + \hat{S}_m^{(z)}\hat{S}_n^{(z)}\hat{S}_m^{(y)}\hat{S}_n^{(y)} \\
&= 3\frac{1}{16}\hat{I} - \frac{1}{4}\left(\hat{S}_m^{(z)}\hat{S}_n^{(z)} + \hat{S}_m^{(y)}\hat{S}_n^{(y)} + \hat{S}_m^{(z)}\hat{S}_n^{(z)} + \hat{S}_m^{(x)}\hat{S}_n^{(x)} + \hat{S}_m^{(y)}\hat{S}_n^{(y)} + \hat{S}_m^{(x)}\hat{S}_n^{(x)}\right) \\
&= \frac{3}{16}\hat{I} - \frac{1}{2}\left(\hat{\mathbf{S}}_m \cdot \hat{\mathbf{S}}_n\right)
\end{aligned} \tag{A1}$$

In the above we used $\left(\hat{S}_m^{(x)}\right)^2 = \left(\hat{S}_m^{(y)}\right)^2 = \left(\hat{S}_m^{(z)}\right)^2 = \frac{1}{4}\hat{I}$ and $\hat{S}_m^{(x)}\hat{S}_m^{(y)} = \frac{i}{2}\hat{S}_m^{(z)} = -\hat{S}_m^{(y)}\hat{S}_m^{(x)}$ (and all cyclic permutations). For $n \neq m$ all spin operators as well as their components commute.

## APPENDIX B: DIAGONALIZATION OF THE SPIN HAMILTONIAN INCLUDING DZYALOSHINKSII-MORIYA INTERACTION

Once we include the Dzyaloshinksii-Moriya interaction it is no longer possible to analytically diagonalize Eq. (5). We proceed as follows. First we diagonalize Eq. (5) including only the bilinear terms (be reminded that the biquadratic terms can be included by using effective bilinear terms, see Appendix I). Then we transform the Dzyaloshinskii-Moriya matrix to the new basis. Note that there are interactions only between electrons along the side of the square (or rhombus) and that the magnitude of all

interactions is taken equal to $\xi$. The transition matrix elements are

$$H^{(DM)} = \xi \left(\begin{array}{ccccc|ccccc|ccccc}
0 & 0 & 0 & 0 & 0 & 0 & 0 & 0 & 0 & 0 & 0 & 0 & 0 & 0 & 0 \\
0 & 0 & 0 & 0 & 0 & \frac{i}{2} & 0 & 0 & 0 & \frac{i}{2\sqrt{2}} & \frac{i}{2\sqrt{2}} & 0 & 0 & 0 & 0 & 0 \\
0 & 0 & 0 & 0 & 0 & 0 & \frac{i}{\sqrt{3}} & 0 & 0 & 0 & 0 & \frac{i}{\sqrt{3}} & 0 & 0 & 0 & 0 \\
0 & 0 & 0 & 0 & 0 & 0 & 0 & \frac{i}{2} & 0 & 0 & 0 & 0 & 0 & \frac{i}{2\sqrt{2}} & \frac{i}{2\sqrt{2}} & 0 \\
0 & 0 & 0 & 0 & 0 & 0 & 0 & 0 & 0 & 0 & 0 & 0 & 0 & 0 & 0 & 0 \\
\hline
0 & -\frac{i}{2} & 0 & 0 & 0 & 0 & 0 & 0 & 0 & -\frac{i}{2\sqrt{2}} & \frac{i}{2\sqrt{2}} & 0 & 0 & 0 & 0 & 0 \\
0 & 0 & -\frac{i}{\sqrt{3}} & 0 & 0 & 0 & 0 & 0 & -\frac{i}{\sqrt{6}} & 0 & 0 & 0 & 0 & 0 & 0 & \frac{i}{\sqrt{2}} \\
0 & 0 & 0 & -\frac{i}{2} & 0 & 0 & 0 & 0 & 0 & 0 & 0 & 0 & 0 & -\frac{i}{2\sqrt{2}} & \frac{i}{2\sqrt{2}} & 0 \\
\hline
0 & 0 & 0 & 0 & 0 & 0 & \frac{i}{\sqrt{6}} & 0 & 0 & 0 & 0 & -i\sqrt{\frac{2}{3}} & 0 & 0 & 0 & 0 \\
0 & -\frac{i}{2\sqrt{2}} & 0 & 0 & 0 & \frac{i}{2\sqrt{2}} & 0 & 0 & 0 & 0 & -\frac{i}{2} & 0 & 0 & 0 & 0 & 0 \\
0 & -\frac{i}{2\sqrt{2}} & 0 & 0 & 0 & -\frac{i}{2\sqrt{2}} & 0 & 0 & 0 & \frac{i}{2} & 0 & 0 & 0 & 0 & 0 & 0 \\
0 & 0 & -\frac{i}{\sqrt{3}} & 0 & 0 & 0 & 0 & 0 & i\sqrt{\frac{2}{3}} & 0 & 0 & 0 & 0 & 0 & 0 & 0 \\
0 & 0 & 0 & 0 & 0 & 0 & 0 & 0 & 0 & 0 & 0 & 0 & 0 & 0 & 0 & 0 \\
0 & 0 & 0 & -\frac{i}{2\sqrt{2}} & 0 & 0 & 0 & \frac{i}{2\sqrt{2}} & 0 & 0 & 0 & 0 & 0 & 0 & -\frac{i}{2} & 0 \\
0 & 0 & 0 & -\frac{i}{2\sqrt{2}} & 0 & 0 & 0 & -\frac{i}{2\sqrt{2}} & 0 & 0 & 0 & 0 & 0 & \frac{i}{2} & 0 & 0 \\
0 & 0 & 0 & 0 & 0 & 0 & -\frac{i}{\sqrt{2}} & 0 & 0 & 0 & 0 & 0 & 0 & 0 & 0 & 0
\end{array}\right) \tag{B1}$$

The blocks in the diagonal indicate groups of degenerate states. Since there are no diagonal elements we must use at least second-order perturbation theory, which, however, is applicable only in the case of nondegenerate interacting states.

$$E_m^{(DM)} = \sum_{n \neq m} \frac{\left|\langle m|\hat{H}^{(DM)}|n\rangle\right|^2}{E_n - E_m}, \tag{B2}$$

where $E_m^{(DM)}$ is the Dzyaloshinskii-Moriya energy correction to the state $|m\rangle$, and $E_m$ and $E_n$ are the zeroth-order energies of states $|m\rangle$ and $|n\rangle$, respectively.

The $6 \times 6$ sub-block (the two degenerate triplet states with energies $J_1 + J_2$) is not a zero block (there are interactions among degenerate states), so we must first diagonalize it. Doing so divides this $6 \times 6$ block into three $2 \times 2$ zero blocks with energies $J_1 + J_2 - \frac{\xi}{2}$, $J_1 + J_2$, and $J_1 + J_2 + \frac{\xi}{2}$. Subsequently, we can safely apply second-order perturbation theory. Since we neglect third-order terms, it makes no sense to include contributions higher than the ones quadratic in $\xi$, because some part of them would not be taken into account. Therefore we perform a Taylor series expansion of the energy corrections up to $\xi^2$. The final results are shown in the last column of Table II, where we see that terms linear to $\xi$ indeed exist only within the subspace of the two degenerate triplets. This procedure of diagonalizing within the $6 \times 6$ subspace is not necessary in rhombic structures, since then the two triplets are not degenerate anymore.

## APPENDIX C: SPIN HAMILTONIAN WITH TWO ELECTRONS PER SITE

For the sake of completeness in Table VI we also give the energies for a perfect square in the case of two electrons per site. The intrasite coupling is $J_0$. Although a $Ni_4$ structure could in principle exhibit a similar level scheme (due to the $d^8$ configuration of the Ni atoms), it turns out that this is not the case. The reason is that the Ni atoms also build chemical bonds at distances below 5 Å (or in a more solid-state parlance one sees the onset of electronic bands). Since a spin Hamiltonian does not take into account the spatial degrees of freedom (there are altogether $4 \times 5 = 20$ $d$ orbitals, not counting the spin), which lift the orbital degeneracies, we end up with unphysically high spins (no net ground state). Note also that "two electrons per site" is not tantamount to "a triplet state per site," due to two reasons: (a) can also produce a singlet state (and hence a richer spectrum), and (b) the triplet-relevant SU(3) Lie group has a higher dimension (eight) than the doublet-relevant SU(2) group (three), and as a consequence it is not possible to simply map biquadratic terms on bilinear ones. This, in turn, means that the biquadratic exchange interactions cannot be rewritten by means of effective bilinear interactions [73].


[1] B. Behin-Aein, D. Datta, S. Salahuddin, and S. Datta, Nat. Nano. **5**, 266 (2010).

[2] A. Khajetoorians, J. Wiebe, B. Chilian, and R. Wiesendanger, Science **332**, 1062 (2011).

[3] I. Žutić and M. Fuhrer, Nat. Phys. **1**, 85 (2005).

[4] S. A. Wolf, Science **294**, 1488 (2001).

[5] S. Maekawa and T. Shinjo, *Spin Dependent Transport in Magnetic Nanostructures* (Taylor & Francis, New York, 2002).

[6] S. Parkin, X. Jiang, C. Kaiser, A. Panchula, K. Roche, and M. Samant, Proc. IEEE **91**, 661 (2003).
[7] C. Joachim, Nanotechnology **13**, R1 (2002).
[8] A. J. Heinrich, C. P. Lutz, J. A. Gupta, and D. M. Eigler, Science **298**, 1381 (2002).
[9] W.-H. Soe, C. Manzano, A. De Sarkar, F. Ample, N. Chandrasekhar, N. Renaud, P. de Mendoza, A. M. Echavarren, M. Hliwa, and C. Joachim, Phys. Rev. B **83**, 155443 (2011).
[10] S. X. Wang, J. Labaziewicz, Y. Ge, R. Shewmon, and I. L. Chuang, Phys. Rev. A **81**, 062332 (2010).
[11] S. Bellucci and P. Onorato, Phys. Rev. B **81**, 165427 (2010).
[12] N. Renaud and C. Joachim, Phys. Rev. A **78**, 062316 (2008).
[13] C. Menzel-Jones and M. Shapiro, Phys. Rev. A **75**, 052308 (2007).
[14] S. Lloyd, Phys. Rev. Lett. **75**, 346 (1995).
[15] L. Wang and B. Li, Phys. Rev. Lett. **99**, 177208 (2007).
[16] C. Ospelkaus, C. E. Langer, J. M. Amini, K. R. Brown, D. Leibfried, and D. J. Wineland, Phys. Rev. Lett. **101**, 090502 (2008).
[17] L.-A. Wu, D. A. Lidar, and M. Friesen, Phys. Rev. Lett. **93**, 030501 (2004).
[18] C. Monroe, D. M. Meekhof, B. E. King, W. M. Itano, and D. J. Wineland, Phys. Rev. Lett. **75**, 4714 (1995).
[19] G. K. Brennen, C. M. Caves, P. S. Jessen, and I. H. Deutsch, Phys. Rev. Lett. **82**, 1060 (1999).
[20] A. Barenco, D. Deutsch, A. Ekert, and R. Jozsa, Phys. Rev. Lett. **74**, 4083 (1995).
[21] W. Hübner, S. Kersten, and G. Lefkidis, Phys. Rev. B **79**, 184431 (2009).
[22] D. Chaudhuri, H. P. Xiang, G. Lefkidis, and W. Hübner, Phys. Rev. B **90**, 245113 (2014).
[23] H. P. Xiang, G. Lefkidis, and W. Hübner, J. Supercond. Nov. Magn. **26**, 2001 (2014).
[24] W. Jin, C. Li, G. Lefkidis, and W. Hübner, Phys. Rev. B **89**, 024419 (2014).
[25] T. Hartenstein, C. Li, G. Lefkidis, and W. Hübner, J. Phys. D: Appl. Phys. **41**, 164006 (2008).
[26] D. Chaudhuri, W. Jin, G. Lefkidis, and W. Hübner, J. Chem. Phys. **143**, 174303 (2015).
[27] C. Li, W. Jin, H. Xiang, G. Lefkidis, and W. Hübner, Phys. Rev. B **84**, 054415 (2011).
[28] C. Li, S. Zhang, W. Jin, G. Lefkidis, and W. Hübner, Phys. Rev. B **89**, 184404 (2014).
[29] C. Li, J. Liu, S. Zhang, G. Lefkidis, and W. Hübner, Carbon **87**, 153 (2015).
[30] W. Jin, F. Rupp, K. Chevalier, M. M. N. Wolf, M. C. Rojas, G. Lefkidis, H.-J. Krüger, R. Diller, and W. Hübner, Phys. Rev. Lett. **109**, 267209 (2012).
[31] W. Jin, M. Becherer, D. Bellaire, G. Lefkidis, M. Gerhards, and W. Hübner, Phys. Rev. B **89**, 144409 (2014).
[32] L. Xiao and L. Wang, J. Phys. Chem. A **108**, 8605 (2004).
[33] J. Kolehmainen, H. Häkkinen, and M. Manninen, Z. Phys. D **40**, 306 (1997).
[34] P. Jakob, K. Anhut, S. Schnur, and A. Groß, Phys. Rev. Lett. **101**, 206101 (2008).
[35] H. Xiang, G. Lefkidis, and W. Hübner, Phys. Rev. B **86**, 134402 (2012).
[36] C. D. Dong, G. Lefkidis, and W. Hübner, Phys. Rev. B **88**, 214421 (2013).
[37] G. Pal, G. Lefkidis, and W. Hübner, J. Phys. Chem. A **113**, 12071 (2009).
[38] G. Pal, G. Lefkidis, H. C. Schneider, and W. Hübner, J. Chem. Phys. **133**, 154309 (2010).
[39] G. P. Zhang, G. Lefkidis, W. Hübner, and Y. Bai, J. Appl. Phys. **109**, 07D303 (2011).
[40] D. Chaudhuri, G. Lefkidis, A. Kubas, K. Fink, and W. Hübner, Springer Proc. Phys. **159**, 159 (2015).
[41] A. I. Krylov, Annu. Rev. Phys. Chem. **59**, 433 (2008).
[42] N. Kirchner, J. van Slageren, B. Tsukerblat, O. Waldmann, and M. Dressel, Phys. Rev. B **78**, 094426 (2008).
[43] P. St. Petkov, G. N. Vayssilov, S. Krüger, and N. Rösch, Phys. Chem. Chem. Phys. **8**, 1282 (2006).
[44] X. López, M.-Y. Huang, G.-C. Huang, S.-M. Peng, F.-Y. Li, M. Bénard, and M.-M. Rohmer, Inorg. Chem. **45**, 9075 (2006).
[45] M. Fondo, N. Ocampo, A. M. García-Deibe, R. Vicente, M. Corbella, M. R. Bermejo, and J. Sanmartín, Inorg. Chem. **45**, 255 (2006).
[46] M. H. Güven and M. Eryürek, Phys. Status Solidi B **213**, 283 (1999).
[47] W. R. Wadt and P. J. Hay, J. Chem. Phys. **82**, 284 (1985).
[48] H. Nakatsuji, Chem. Phys. Lett. **67**, 329 (1979).
[49] M. J. Frisch, G. W. Trucks, H. B. Schlegel, G. E. Scuseria, M. A. Robb, J. R. Cheeseman, G. Scalmani, V. Barone, B. Mennucci, G. A. Petersson *et al.*, Gaussian 09 Revision D.01, Gaussian Inc., Wallingford, CT, 2009.
[50] L. Peters, I. Di Marco, O. Grånäs, E. Şaşıoğlu, A. Altun, S. Rossen, C. Friedrich, S. Blügel, M. I. Katsnelson, A. Kirilyuk *et al.*, Phys. Rev. B **93**, 224428 (2016).
[51] A. Szabo and N. S. Ostlund, *Modern Quantum Chemistry: Introduction to Advanced Electronic Structure Theory* (Dover Publications, Mineola, NY, 1996).
[52] G. Lefkidis, *Nanoscience and Computational Chemistry: Research Progress*, edited by A. G. Mercader, E. A. Castro, and A. K. Haghi (Apple Academic Press, Toronto, New Jersey, 2013), Chap. 4.
[53] R. Gómez-Abal, O. Ney, K. Satitkovitchai, and W. Hübner, Phys. Rev. Lett. **92**, 227402 (2004).
[54] G. Lefkidis, G. P. Zhang, and W. Hübner, Phys. Rev. Lett. **103**, 217401 (2009).
[55] G. Lefkidis and W. Hübner, Phys. Rev. B **87**, 014404 (2013).
[56] R. R. Cash and A. H. Karp, ACM Trans. Math. Software **16**, 201 (1990).
[57] R. Skomski, *Simple Models of Magnetism* (Oxford University Press, New York, 2008).
[58] T. Moriya, Phys. Rev. **120**, 91 (1960).
[59] H. A. Brown, Phys. Rev. B **4**, 115 (1971).
[60] W. Hübner and L. M. Falicov, Phys. Rev. B **47**, 8783 (1993).
[61] D. E. Eastman, F. J. Himpsel, and J. A. Knapp, Phys. Rev. Lett. **44**, 95 (1980).
[62] The importance of the orbital degree of freedom for the *d-d* exchange interaction will be published elsewhere.
[63] G. P. Zhang, Y. H. Bai, and T. F. George, J. Phys.: Condens. Matter **28**, 236004 (2016).
[64] R. V. Mikhaylovskiy, E. Hendry, A. Secchi, J. H. Mentink, M. Eckstein, A. Wu, R. V. Pisarev, V. V. Kruglyak, M. I. Katsnelson, T. Rasing *et al.*, Nat. Commun. **6**, 8190 (2015).
[65] G. Lefkidis and W. Hübner, Phys. Rev. B **76**, 014418 (2007).
[66] G. P. Zhang, W. Hübner, G. Lefkidis, Y. Bai, and T. F. George, Nat. Phys. **5**, 499 (2009).

[67] E. Fredkin and T. Toffoli, Int. J. Theor. Phys. **21**, 219 (1982).
[68] D. P. DiVincenzo, Fortschr. Phys. **48**, 771 (2000).
[69] W. Wernsdorfer and L. Bogani, Nat. Mater. **7**, 179 (2008).
[70] A. Ardavan, O. Rival, J. J. L. Morton, S. J. Blundell, A. M. Tyryshkin, G. A. Timco, and R. E. P. Winpenny, Phys. Rev. Lett. **98**, 057201 (2007).
[71] B.-G. Englert, Phys. Rev. Lett. **77**, 2154 (1996).
[72] J. T. Haraldsen, T. Barnes, and J. L. Musfeldt, Phys. Rev. B **71**, 064403 (2005).
[73] D. A. Varshalovich, A. N. Moskalev, and V. K. Khersonsky, *Quantum Theory of Angular Momentum* (World Scientific, Singapore, 1988).